Accurate Characterization by Dielectric Spectroscopy up to 25 GHz of Nano-Liter Range Liquid Volume Within a Microfluidic Channel

Houssein Mariam, Patrick Poulichet, Hakim Takhedmit, Frederique Deshours, Elodie Richalot, Olivier Francais

▶ **To cite this version:**

Houssein Mariam, Patrick Poulichet, Hakim Takhedmit, Frederique Deshours, Elodie Richalot, et al.. Accurate Characterization by Dielectric Spectroscopy up to 25 GHz of Nano-Liter Range Liquid Volume Within a Microfluidic Channel. IEEE Sensors Journal, 2022, 22 (4), pp.3553-3564. 10.1109/JSEN.2021.3138771 . hal-04243706

HAL Id: hal-04243706
https://hal.science/hal-04243706

Submitted on 30 Jan 2024

HAL is a multi-disciplinary open access archive for the deposit and dissemination of scientific research documents, whether they are published or not. The documents may come from teaching and research institutions in France or abroad, or from public or private research centers.

L'archive ouverte pluridisciplinaire **HAL**, est destinée au dépôt et à la diffusion de documents scientifiques de niveau recherche, publiés ou non, émanant des établissements d'enseignement et de recherche français ou étrangers, des laboratoires publics ou privés.

Accurate Characterization by Dielectric Spectroscopy up to 25 GHz of Nano-liter Range Liquid Volume within a Microfluidic Channel

Houssein Mariam, Patrick Poulichet, Hakim Takhedmit, Frédérique Deshours, Elodie Richalot and Olivier Français

***Abstract*— This paper reports the design, simulation and experimental validation of an accurate liquid sensing technique in the nano-liter range. It is suitable for the detection and quantification of very small contents of liquid samples containing biological cells. The biosensor is based on an open-ended interdigitated capacitor (IDC) within a microfluidic channel. The microwave structure including the IDC is patterned in coplanar waveguide technology. The microfluidic channel is 100 µm thick and the IDC covers an area of 150 µm width and 90 µm length. This leads to a volume under analysis much lower than a nano-liter which allows the noninvasive and contactless microwave investigation of biological cells in their culture medium. This micro-device is used to extract the complex permittivity of liquid media from the measured scattering parameters within the frequency band ranging from 0.2 to 25 GHz. For ease of use, a SMA-connectorized version of the device with spring contacts probes to the biosensor is also proposed. Results concerning microparticle detection within the media are also presented, extending the use of the sensors to cellular environments.**

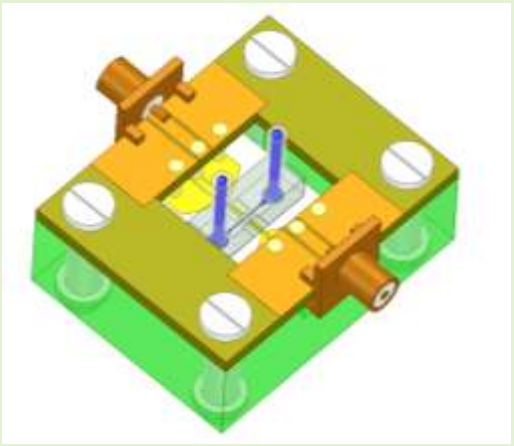

***Index Terms*— Complex permittivity, Coplanar waveguide InterDigitated Capacitor, Dielectric spectroscopy, Microfluidic.**

I. Introduction

Microwave dielectric spectroscopy technique has attracted interest for applications in chemistry, biochemistry, biology and medicine [1]. With the help of micro-technologies, it is possible to develop miniaturized biosensor dedicated to the analysis of liquid and/or biological media based on this principle [2]. The characterization of materials by dielectric spectroscopy using frequency reflectometry is a well-known method allowing the characterization of homogeneous, inhomogeneous and/or porous media (concrete, biological media, etc.). Several technologies are presented in the literature; they are based on different analysis methods operated in a certain frequency range and over a considered sensitive zone (analysis volume) [3-4]. Based on this principle, the development of new cellular and molecular analyzing instruments opens new and innovative ways for non-invasive cell analysis and real-time monitoring.

Houssein Mariam, Hakim Takhedmit and Elodie Richalot are with ESYCOM lab, Univ Gustave Eiffel, CNRS UMR 9007, F-77454 Marne-la-Vallee, France (e-mail: hsein.mariam@gmail.com; hakim.takhedmit@univeiffel.fr; elodie.richalot-taisne@univ-eiffel.fr).
Patrick Poulichet and Olivier Français are with the ESYCOM lab, Univ Gustave Eiffel, ESIEE Paris, F-93160 Noisy-le-Grand (e-mail: p.poulichet@esiee.fr; olivier.francais@esiee.fr).
Frédéric Deshours is with GEEPS lab, Sorbonne Université, Paris, France (e-mail: frederique.deshours@sorbonne-universite.fr.

In this paper, two homemade structures based on a coplanar waveguide technology and operating in reflection mode are presented: the first probe is based on an open-ended (OE) line and the second probe is based on an interdigitated capacitor (IDC). These sensors are studied through simulations using HFSS (High Frequency Structure Simulator) software from Ansoft, fabricated with microtechnology process and used for dielectric characterization of liquid media. The results show that the two sensor types enable an accurate determination of the frequency dependence of the complex permittivity.

In order to understand the extraction principles of the complex dielectric permittivity of materials, a first macro-sensor was designed and simulated before addressing micro-sensors. Its simple shape corresponds to an open-ended coaxial probe associated to a circular coppered ground (Fig.1). Open-line Coaxial probes (OC) are widely used for microwave dielectric spectroscopy in different fields [5-18]. According to simulation results, the sensitive region is roughly a cylinder centered at the open-ended cable core with a radius of approximately 8 mm and a height of 7 mm. Thus, this probe operates in the milliliter range, which requires a large volume of liquid for sufficient accuracy and is not suitable to target a small number of cells.

Reducing the size of the sensitive area using micro-sensors offers the opportunity to analyze samples containing biological cells, and to examine, at the cell scale, the dielectric properties of cells in regards to potential pathologies (cell

XXXX-XXXX © XXXX IEEE. Personal use is permitted, but republication/redistribution requires IEEE permission.
See http://www.ieee.org/publications_standards/publications/rights/index.html for more information.

type, cancer cell, anemia, etc.). There are some major publications in the field of miniaturized RF sensors dedicated to bioengineering. [19] uses microtechnology to fabricate a biologic sensor connected by RF probes and based on a transmission line with a volume under test of around 3 µL. Measurement of fluid properties can be done up to 40 GHz with de-embedding technique to take into account both the CPW accesses as well as the polymer walls of the fluidic channel. In [20] and [21], IDC (Interdigitated Capacitor) is then used to detect the permittivity of the fluid by measuring the transmission parameter (S_{21}). The sensing volume of liquid is about 1 nL. To ensure a good sensitivity of the detection of the permittivity of the analyzed fluid, de-embedding procedure is applied to subtract the effect of the coplanar access lines. The sensor is tested with different binary liquid mixtures. Living B lymphoma cells was also tested.

Table I summarizes the state of the art concerning micro-devices based on electromagnetic characterization (using S_{11} or S_{21} parameters) of biological species (liquids, particles, cells) over a broadband range.

Compared to the state of the art, this paper is based on reflexing approach (S_{11}), as only one port is needed which simplifies the use of the sensor. To make it even easier to use, a packaged chip with a SMA connector associated to spring contact probes is presented for the first time. It offers increased portability (avoiding the use of RF probes) and also enables the change of the sensor for each analysis, while keeping the same packaging.

In addition, from the reflection coefficient measurement of the MUT (Medium Under Test), an algorithm using three reference media [3] is developed. The complex permittivity of the sample is then extracted and compared to the theoretical modeling.

The design presented in this paper uses a coplanar-waveguide (CPW) which consists of an open-ended probe combined with a micro-fluidic channel. The proposed sensor, presented in Fig. 1, is used to characterize a liquid flowing within a microfluidic channel located at the end of the CPW line. The MUT corresponds to an analyzed volume in the nanoliter scale. This makes it suitable for measurement of one or a few biological cells, in a non-invasive way, in their liquid culture medium in order to extract their specific dielectric properties. This device was used for broadband determination of the dielectric properties of liquids and mixtures of water and methanol in the frequency range 200 MHz – 25 GHz.

The comparison of our sensor to the state-of-the art is provided in table I.

The purpose of this paper is to investigate the viability of using an interdigitated device for dielectric spectroscopy of small liquid volume as a tool for biological analysis compatible with microfluidic devices. The technique proposed here is based on the analysis of the reflection coefficient S_{11}. The electromagnetic field at the open-ended CPW probe aperture interacts with the sample at the interface, between the end of the line and the medium under test, in a manner that it depends on the dielectric properties of the medium. Thus, the complex relative permittivity (ε_r^*) of the unknown sample can be extracted from the reflection coefficient (S_{11}); this permittivity extraction is performed by using the technique proposed by Wagner et *al* [3].

TABLE I
STATE OF THE ART COMPARISON TABLE

Reference	Frequency	S parameter / measurement technique	Extracted characteristic	MUT (liquids, particles, cells …)
[22]	0.1 GHz to 10 GHz	On-chip sensor FFT applied on Baseband signal	Complex permittivity - Permittivity imaging (matrix of patchs)	Liquids - µL range
[20], [21]	Up to 40 GHz	Transmission mode (S21) - Probe station	Relative permittivity	HEK-293 biological cells in suspension (more than 20 cells) - nL range
[19]	Up to 40 GHz	Transmission (S21) - Probe station (but also possible using SMA-connectorized)	Relative/effective permittivity	HUVEC cells in suspension in their biological medium (various concentrations and number of cells) - nL range
[23]	1 GHz to 5 GHz	Refection and transmission (S11 and S21) modes - SMA-connectorized	Differences in terms of S11 and S21 compared to reference media	Jurkat and HEK cells (live and dead) in different cultures (from 20 cells) - nL range
[24]	Up to 8 GHz	Transmission mode (S21)	Capacitance contrast - S21 magnitude (dB) - Permittivity	Validated by 1 polystyrene particle. Measurement done using SW-620 cell line (cancerous colorectal cell line) - nL range
[25], [26]	40 MHz to 40 GHz	Transmission mode (S21)	Capacitive and conductive contrasts	Living B lymphoma cell (1 cell) - nL range
[27], [28], [29]	kHz to 9 GHz	2-port sensor - S21 (trans.) for series configuration and S11 (refl.) for shunt configuration - Probe station use	Insertion loss changes - Return loss changes	Live Jurkat cell trapped by dielectrophoresis (1 cell) - nL range
This paper	0.2 GHz to 25 GHz	Reflection (S11) mode - Probe station - SMA-connectorized and spring contact probe (removable packaging)	Complex permittivity	Liquids and polystyrene particles (from 1 particle) - nL range

This paper is organized as follows. Section II is dedicated to the description and simulation of the two different micro-sensors. Section III is dedicated to the measurement procedure, including the calibration step. Section IV deals with the experimental validation of the approach by analyzing the dielectric properties of the measured media under probe, taking into account the calibration procedure and the feasibility of micro-particle detection. Section V concerns a packaged version of the sensor with SMA connectors to offer portability capabilities. It also discusses the experimental results obtained with liquid mixtures based on aqueous solutions, which feature various solute concentrations.

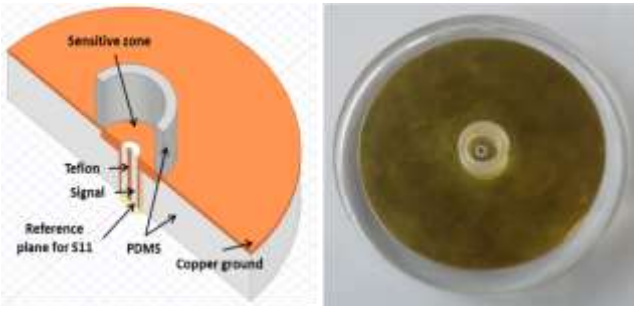

Fig. 1. Homemade open-line coaxial probe structure in 3D view (left) simulated and (right) fabricated.

II. SENSOR DESCRIPTION AND SIMULATIONS

A. Shape and design of the sensor

The proposed micro-sensor is based on an interdigitated capacitor (IDC) located at the end of a coplanar waveguide (Fig. 2). The dielectric detection area, corresponding to the IDC surface covered by under-test liquids, is a rectangle of 150 µm width by 90 µm length. The liquid confinement is assured with a microfluidic channel (width of 150 µm) composed of SU-8 photoresist, which features a height of 100 µm and can be easily down-scaled. This polymer has the main advantages of being biocompatible and easily patterned. Its viscosity facilitates coating of uniform thin films and, later on, removal of non-exposed resin (undesirable) during development step (photolithography process). Its transparency allows an easy observation of the fluidic materials injected in the channel, and notably biological cells.

The IDC presents strips and slots of 10 µm width as presented in Fig. 2. The microwave electrodes are made of a thin layer of titanium (TiW - 20nm) and gold (200nm) on the glass wafer to minimize additional dielectric losses due to the substrate. This structure is compared with a single open-ended (OE) coplanar line depicted in Fig. 3 and presented in [18].

The fabrication of the CPW sensor is based on the use of standard microtechnology processes and may be divided in two main parts: 1) The elaboration of the IDC along with its access line on the glass wafer, 2) The realization of the microfluidic channel. More details about the fabrication steps are given in [30].

The performances of the IDC were investigated using HFSS software to evaluate the electric-field distribution in the sensing area. The electromagnetic field at the open-ended CPW probe extremity fringes into the sample at the interface.

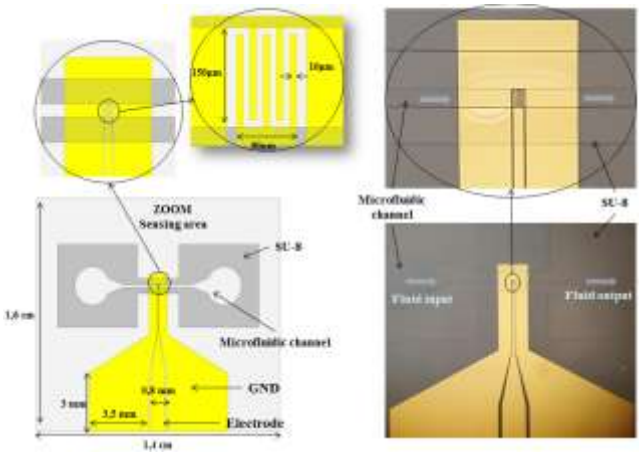

Fig. 2. Interdigitated capacitor structure in top view (left simulated and (right) fabricated.

Fig. 4 presents a view of the electric field calculated for the design developed when loaded by deionized water. The electrical field distribution at 5 GHz is strongly concentrated in the IDC area where the interaction between the electromagnetic wave and the liquid sample indicates a stable sensitive area of approximately 15µm height above the IDC region. Only the liquid volume located in the sensitive area above the sensor end is analyzed by the IDC.

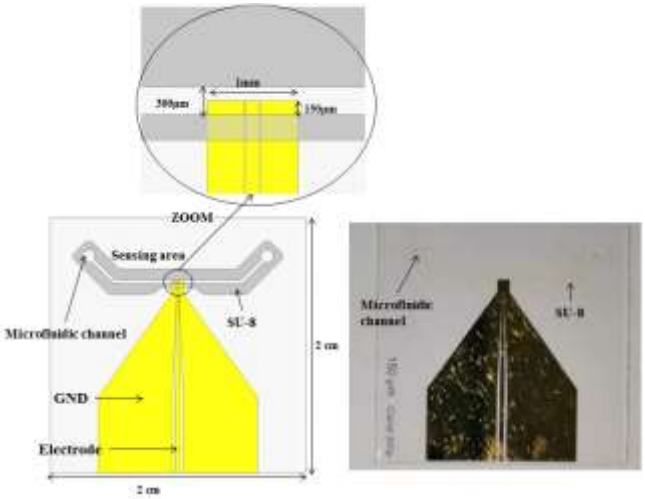

Fig. 3. Open-ended structure in top view: (left) simulated and (right) fabricated.

The CPW line, integrated into the microfluidic channel, was produced by two photolithography steps. The values of IDC capacitance are affected by the width of the fingers constituting the interdigitated capacitor. These fingers are obtained after the development step where the unwanted metallization is removed and the obtained dimensions are associated to a defined accuracy.

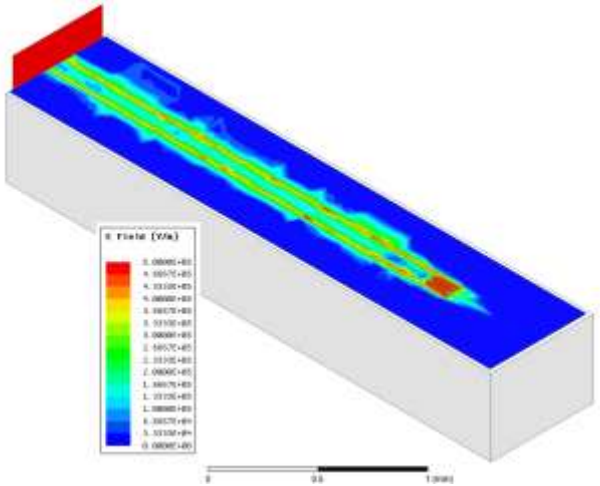

Fig. 4. Simulated distribution ~~at the sensor-liquid~~ of the electric-field magnitude when the sensor ~~IDC~~ is loaded with deionized water at 5 GHz.

B. Estimated behavior of the sensor

To evaluate the impact on the sensor performances of these size inaccuracies, simulations were carried out using HFSS for capacitances of different finger widths (8µm, 9µm 9.5µm, 9.7µm, 9.8µm, 9.9µm and 10µm). Fig. 5 shows the capacitive contrast between the extracted capacitances when considering sensor loaded by water and air. It shows a lower sensitivity when the width deviates from 10 µm; However, the fabrication uncertainties are taken into account and corrected during the calibration step.

To perform under-probe measurements, a suitable coplanar access is developed as presented in Fig 6. The capacitive effect for both OE and IDC geometries were estimated and compared according to the shape of the aperture at the reference plane for the extracted input-impedance Z_{11}. Likewise, the capacitive contrasts between the extracted capacitances when considering sensors loaded by water and ethanol was calculated.

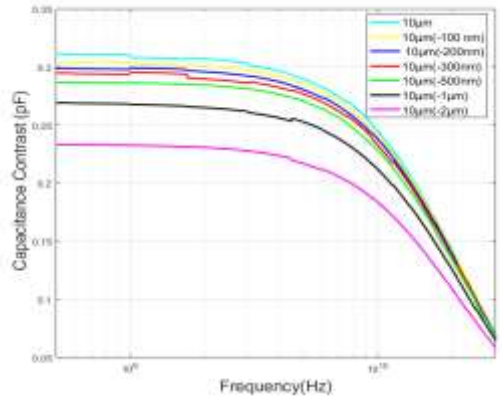

Fig. 5. Simulated contrasts of extracted capacitances when IDC-sensor is loaded by water and air, for different finger widths.

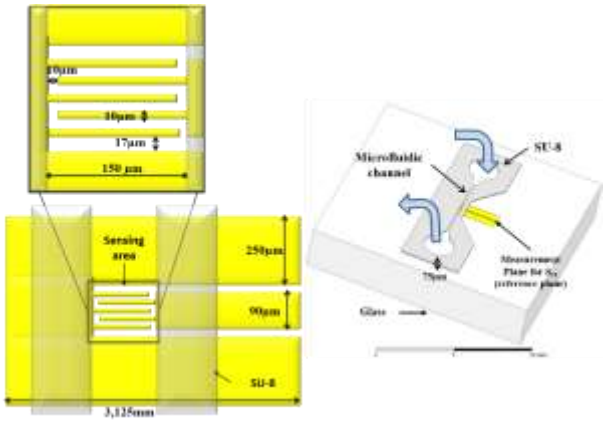

Fig. 6. Simulated Sub-device: In top view (left) and in 3D view (right).

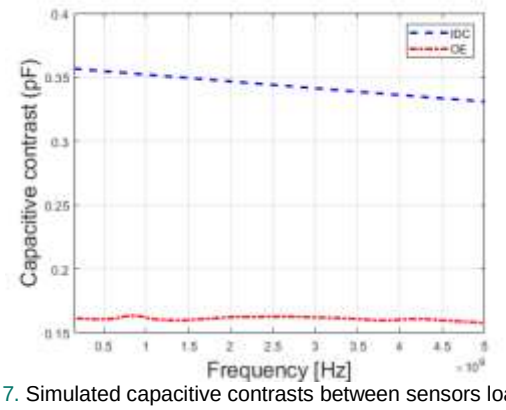

Fig. 7. Simulated capacitive contrasts between sensors loaded by water or air for both geometries.

Fig. 7 shows that the capacitive contrasts obtained using IDC are twice more than those obtained using the OE sensor. This means that the coupling between the interdigitated detection zone and the sample under test is stronger compared to that of an open-ended line. Indeed, the increase of the capacitance value makes it possible to estimate in a more sensitive way the values of complex relative permittivity of materials.

Based on these two considered designs, protocol for extracting dielectric parameters for the media under test is defined in Section III.

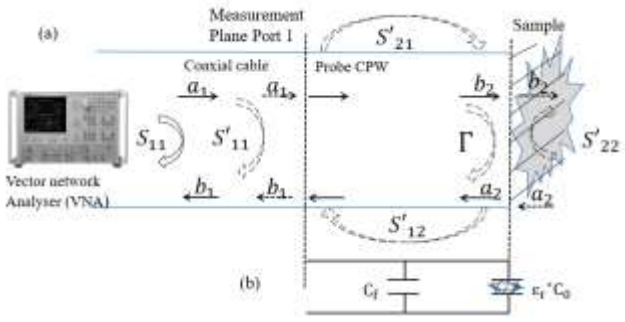

Fig. 8. Schematic diagram of measurement plans and equivalent lumped-element circuit of the CPW tip (sensitive area).

III. MEASUREMENT PROCEDURE

A. Permittivity measurement and extraction setup

The presented method for the determination of the complex dielectric permittivity of materials is based on the interaction between the electromagnetic wave and the liquid within the microfluidic channel. When an electric field is applied on a dielectric material, its atoms are oriented according to the electric field direction. These excited dipoles undergo a relaxation time. The classical model to describe the frequency response of the liquid polarization corresponds to a first-order equation known as the Debye equation which can be written as [31, 32]:

$$\varepsilon_r^* = \varepsilon_\infty + \frac{\varepsilon_s - \varepsilon_\infty}{1 + j\frac{f}{f_r}} \quad (1)$$

where ε_s is the static permittivity, ε_∞ is the high frequency permittivity at infinite frequency and f_r is the relaxation frequency.

The schematic diagram of the measurement plans and an appropriate lumped-element equivalent circuit of the CPW-tip sensor (sensitive area) are shown in Fig. 8.

The effect of the access line under the micro-channel wall is represented by the capacitor C_f. The capacitor C_0 represents a detection capacitance and depends on the coupling between the fields and the sample through its complex permittivity ε_r^*. The relationship between this complex permittivity ε_r^* and the complex reflection coefficient Γ at the interface between the end of the CPW probe and the sample is given by the following equation:

$$\varepsilon_r^* = \frac{1}{j\omega z_0 C_0}\frac{1-\Gamma}{1+\Gamma} - \frac{C_f}{C_0} \quad (2)$$

When the microfluidic channel is loaded by a fluid medium of complex permittivity ε_r^*, the complex impedance Z_{eq}^*, representing the sensor tip, changes and is given by the following expression:

$$Z_{eq}^* = \left(j\omega C_f + j\omega\varepsilon_r^* C_0\right)^{-1} \quad (3)$$

The reflection coefficient Γ at the interface between the end of the biosensor and the liquid under test is related to the equivalent complex impedance Z_{eq}^* according to:

$$Z_{eq}^* = \frac{1}{Y^*} = z_0\frac{1-\Gamma}{1+\Gamma} \quad (4)$$

The characterization method consists in measuring using a vector network analyzer (VNA) the parameters S_{11} of the circuit loaded by different materials. The scattering matrix [S'] of a structure is given by:

$$\begin{pmatrix} b_1 \\ b_2 \end{pmatrix} = \begin{pmatrix} S'_{11} & S'_{12} \\ S'_{21} & S'_{22} \end{pmatrix}\begin{pmatrix} a_1 \\ a_2 \end{pmatrix} \quad (5)$$

Using the fluence graph of the probe represented in Fig. 8 and the equation (5) with $S_{11} = \frac{b_1}{a1}$ and $\Gamma = \frac{a_2}{b_2}$, it can be deduced:

$$S_{11} = S'_{11} + S'_{12}\frac{a_2}{a_1} \quad \text{and} \quad \Gamma = \frac{S_{11} - S'_{11}}{S'_{22}S_{11} - detS'} \quad (6)$$

By combining (2), (3) and (4), the following bilinear equations can be obtained between measured reflection coefficient S_{11} and complex relative permittivity ε_r^* [33], [34]:

$$S_{11} = \frac{d_2 + d_3\varepsilon_r^*}{d_1 + \varepsilon_r^*} \quad (7)$$

where d_1, d_2 and d_3 are given by:

$$d_1 = \frac{1 - S'_{22}}{j\omega Z_0 C_0(1+S'_{22})} + \frac{C_f}{C_0} \quad (8)$$

$$d_2 = \frac{S'_{11} - S'_{11}S'_{22} + S'_{12}S'_{21}}{j\omega Z_0 C_0(1+S'_{22})} + \frac{C_f(S'_{11} + S'_{11}S'_{22} - S'_{12}S'_{21})}{C_0(1+S'_{22})} \quad (9)$$

$$d_3 = \frac{S'_{11} + S'_{11}S'_{22} - S'_{12}S'_{21}}{j\omega Z_0 C_0(1+S'_{22})} \quad (10)$$

To be able to calculate the complex calibration constants, a calibration step is required as detailed in the next section.

B. Calibration step

The permittivity extraction technique is based on the exploitation of reflection coefficient S_{11}. A bilinear equation describes the relationship between measured S_{11} and the complex relative permittivity $\varepsilon_r^*(f) = \varepsilon'(f) - j\varepsilon''(f)$ of the sample under characterization given by [33], [34]:

$$\varepsilon_r^* = \frac{d_1 + d_3\varepsilon_r^*}{d_1 + \varepsilon_r^*} \quad (11)$$

where d_1, d_2 and d_3 are three complex constants related to the geometry and constitutive materials of the sensor.

Reference materials are required for calibrating and testing instruments that are used for dielectric properties characterization. Pure liquids, especially alcohol, are good reference materials, as they are perfectly uniform and homogeneous unlike many solid materials. They have the advantage of being readily available commercially. If they are sufficiently homogeneous, their properties vary slightly from one sample to another.

Eq. (11) describes the relationship between the complex permittivity and the measured reflection coefficient S_{11} of the MUT. According to this equation, a calibration step with at least three reference media of well-known behavior from the literature is required to be able to calculate the complex calibration constants d_i (i = 1, 2, 3). The media suggested for this calibration step are air ($\varepsilon_{r,O}^* = 1, S_{ij} = S_{ij}^O$), deionized water ($\varepsilon_r^* = \varepsilon_{r,W}^*, S_{11} = S_{11}^W$) and another third medium ($\varepsilon_r^* = \varepsilon_{r,L}^*, S_{11} = S_{11}^L$).

Thus, according to equation (11), the relations (12), (13) and (14) are obtained:

$$\boldsymbol{S_{11}^{O} d_1, -d_2 - \varepsilon_{r,O}^{*} d_3 = -\varepsilon_{r,O}^{*} S_{11}^{O}} \quad (12)$$

$$\boldsymbol{S_{11}^{W} d_1 - d_2 - \varepsilon_{r,W}^{*} d_3 = -\varepsilon_{r,W}^{*} S_{11}^{W}} \quad (13)$$

$$\boldsymbol{S_{11}^{L} d_1 - d_2 - \varepsilon_{r,L}^{*}\ d_3 = -\varepsilon_{r,L}^{*} S_{11}^{L}} \quad (14)$$

These equations can be rewritten in matrix form:

$$\begin{pmatrix} s_{11}^{O} & -1 & -\varepsilon_{r,O}^{*} \\ s_{11}^{W} & -1 & -\varepsilon_{r,W}^{*} \\ s_{11}^{L} & -1 & -\varepsilon_{r,L}^{*} \end{pmatrix} \begin{pmatrix} d_1 \\ d_2 \\ d_3 \end{pmatrix} = \begin{pmatrix} -\varepsilon_{r,O}^{*} s_{11}^{O} \\ -\varepsilon_{r,W}^{*} s_{11}^{W} \\ -\varepsilon_{r,L_1}^{*} s_{11}^{L} \end{pmatrix} \Leftrightarrow Md = e \quad (15)$$

In this case with three known samples, the three constants will be determined numerically by the relation $d = M^{-1}.e$. In case of measurements with more than with three known samples, the inverse of the matrix M must be written as d= $(M^T M)^{-1} M^T.e$ and can be solved numerically. Then, the complex relative permittivity ε_r^* of an unknown sample is directly obtained from measured reflection coefficient S_{11} using Eq. (11).

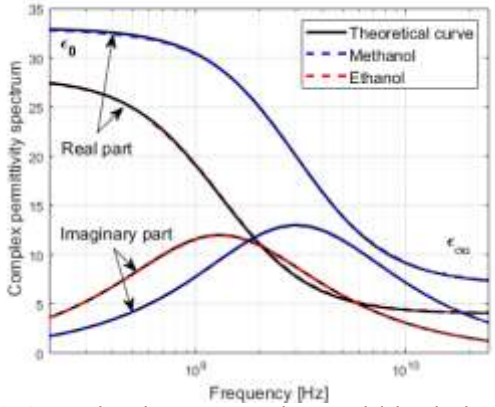

Fig. 9. Comparison between complex permittivity obtained using simulations and those given theoretically by the Debye model.

IV. EXTRACTION AND ANALYSIS OF THE DIELECTRIC PROPERTIES OF THE MEASURED MEDIA

A. Analysis of IDC sensor by numerical simulation and under probe measurements

To validate the parameter extraction process, simulations of the microwave devices, loaded by different tested media with well-known dielectric permittivity, have been performed using the 3D electromagnetic simulator Ansys HFSS. The Debye model of each medium placed within the micro-fluidic channel has been implemented.

Fig. 9 shows the real and imaginary parts of the dielectric permittivity for different media given by the Debye model (theoretical curves). These values are compared with the complex dielectric permittivity extracted from the reflection coefficients S_{11} obtained by simulating the IDC sensor with HFSS software then using eq. (11) after the calibration phase detailed above. The three reference media used are: air, deionized water and acetone. A good concordance is obtained between theoretical and extracted curves.

This shows the relevance of the miniaturized sensor associated with the extraction method used to determine the Debye model of the media under test, over a wide frequency band ranging from 200 MHz to 25 GHz. These results validate the method of analyzing the dielectric properties of the fluids under test, which is based on reflectometry measurements using a CPW line integrated in a microfluidic channel; these results also validate the extraction method of dielectric constants from the measurement and the calibration phase with well-known reference media.

The used experimental setup is shown in Fig. 10. In the first step, the measurement setup is calibrated on one port using Agilent calibration kit (SOL-type). Next, the microsensor, presented above, is characterized under RF probe station through the measure of the reflection coefficients S_{11} when loaded by different fluids (air, deionized water, methanol, ethanol and acetone) as presented in Fig. 11. All measurements throughout this paper have been performed using a vector network analyzer (PNA E8361C from Keysight) and for a power of -10dBm in order to limit sample temperature increase [20].

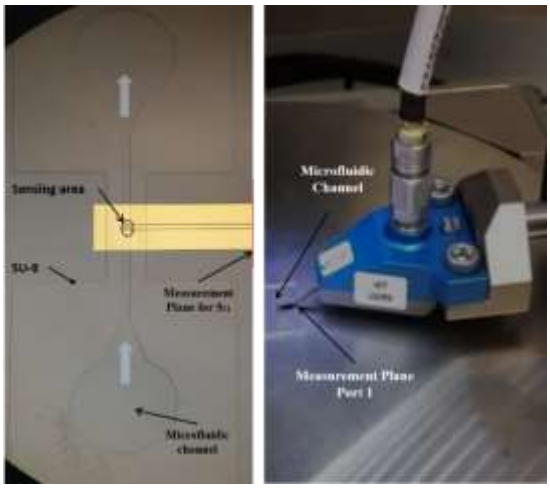

Fig. 10. Fabricated prototype (left) and under probe measurement setup for sensor characterization using Infinity probe (right).

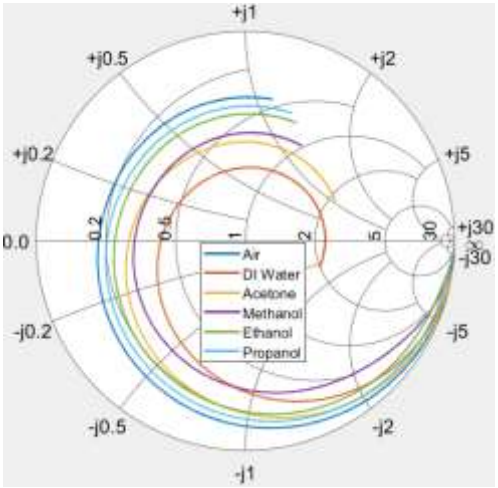

Fig. 11. Smith chart of the S_{11} reflection coefficients measured from 200 MHz to 25 GHz for different liquids in the microfluidic channel.

The Debye equation require three parameters (ε_s, f_r, ε_∞) to describe the frequency-dependent dielectric relaxation behavior of dielectric media. Using the measurement results and the extraction protocol based on the three-calibration media {air, deionized water, acetone}, these dielectric parameters of the complex dielectric permittivity of ethanol are determined. Fig. 12 depicts the dielectric permittivity extracted from the measurement results of pure methanol and ethanol using the sensor depicted in Fig. 6. The extraction is done with curves obtained by adjustment with the scientific calculation software (using of the Matlab® lsqcurvefit function), leading to the closest curves according to least mean square approach that follows the analytical expression of (1).

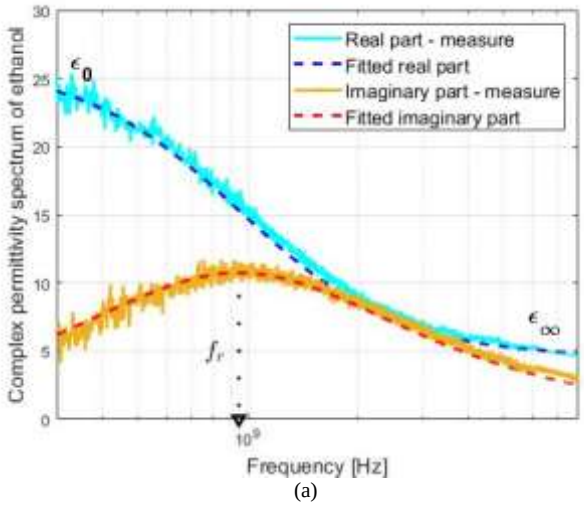

(a)

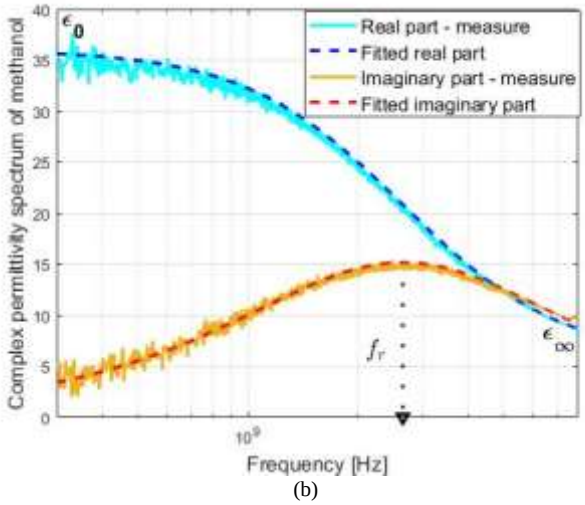

(b)

Fig. 12. Real and imaginary parts of the dielectric permittivity of ethanol (a) and methanol (b) extracted and fitted from measurements.

The values of the high and low frequency relative permittivity and relaxation frequency associated to the fitted curves obtained at 20 °C by adjustment of the extraction results are, for the ethanol $\varepsilon_S^* = 24.77$ (1.56%), $\varepsilon_\infty = 3.89$ (15.17%) and f_r = 0.821 GHz (0.97%), and for the methanol $\varepsilon_S^* = 33.54$ (0.30%), $\varepsilon_\infty = 5.73$ (1.28%) and f_r = 2.64 GHz (6.63%), with between brackets, the differences (in %) compared to the theoretical values.

B. *Influence of the calibration media*

To test the robustness of the method with respect to the choice of reference media for calibration, we carried out the extraction of the properties of media from measurements, when considering different triplets of reference media.

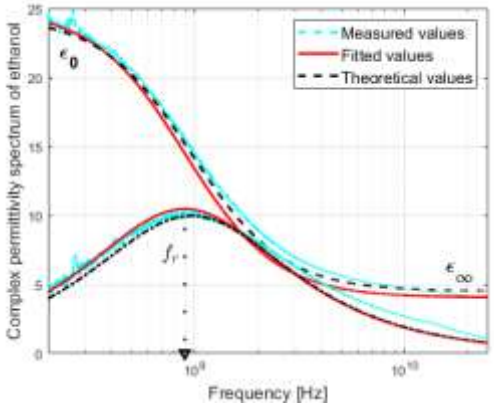

Fig. 13. Real and imaginary parts of the dielectric permittivity of ethanol fitted or extracted from the measurement using the calibration media (air, deionized water, methanol).

Fig. 13 present respectively the dielectric spectra of pure ethanol obtained using 3 calibrations media: Air, deionized water, and methanol. We extract the dielectric characteristics of acetone and ethanol with a good correlation on the frequency behavior in our measurement range (0.2 to 25 GHz).

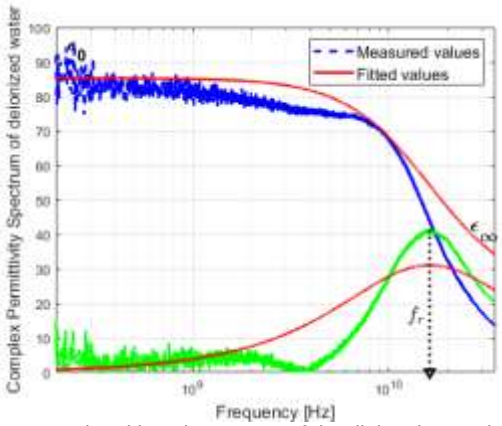

Fig. 14. Real and imaginary parts of the dielectric permittivity of deionized water fitted or extracted from the measurement using the calibration media (air, methanol, acetone).

Using calibration triplet (air, methanol, acetone), the real and imaginary parts of the dielectric permittivity of deionized water has been extracted from measurement and the obtained values have been fitted considering Debye model (Fig. 14).

The real static permittivity of water has a value very far from those of the media used in the calibration step and greatly exceeds the highest static permittivity of the reference media ($\varepsilon_{r,o}^* = 1$ for air, $\varepsilon_{r,o}^*$ =21 for acetone and $\varepsilon_{r,o}^* = 32.66$ for methanol). With measurements, static permittivity of deionized water $\varepsilon_{r,o}^*$ =85.27 obtained is very close to the theoretical one that is 80.21. Likewise, the relaxation frequency estimated from measurement is 16.18 GHz against 17.00 GHz in theory.

C. Detection of micro particles

To test the capability of our sensor to detect the presence of a cell, some measurements have been performed while injecting polystyrene micro particles in water within the channel. For one particle of diameter 20 µm located on the IDC, the dielectric permittivity of the equivalent material within the sensing area has been extracted from measurements and compared to the one of water. Besides, to consolidate this result, simulations have been performed with a sensor loaded by water with one, two and three polystyrene particles on the IDC (Fig. 15).

The difference between water permittivity and the permittivity extracted from measurements or simulations with one or several particles on the IDC is presented in Fig. 16; the order of magnitude of the difference obtained with one single particle is in agreement in simulation and measurement. As expected, this difference between permittivity increases versus the number of inserted particles. These results show that the presence of a few single particles can be detected using this sensor.

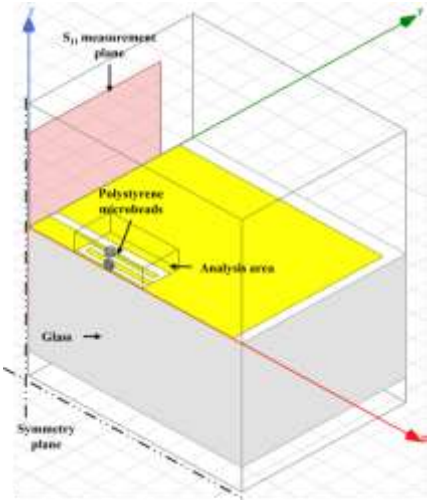

Fig. 15. Simulated IDC sensor loaded by water and three particles. Due to the geometrical symmetry, only the half of the structure is simulated.

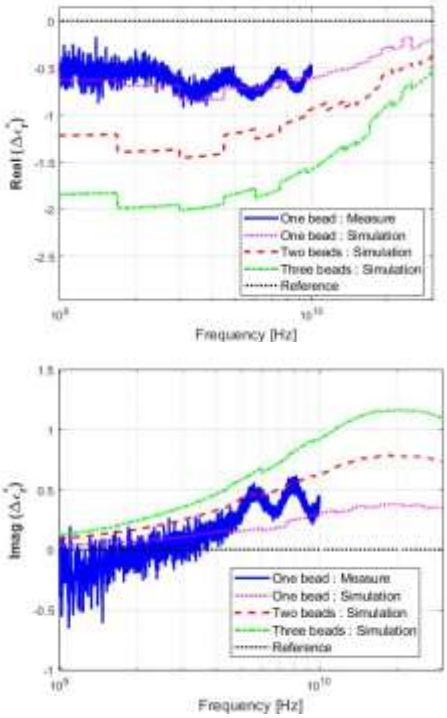

Fig. 16. Real and imaginary parts of the difference between water permittivity and the ones extracted from measurement with one polystyrene particle or simulations with one, two or three particles on the IDC.

V. PACKAGED SENSOR WITH SMA ACCESS

A. Measurements and analysis of the dielectric properties of the measured media with SMA connector

In order to achieve a portable device, the chip presented in Fig. 2 was packaged with a SMA connector on a PCB support as shown Fig. 17. A mechanical support has been fabricated by an additive technique to maintain the microstructure, and three spring loaded contacts ensure the electrical continuity between the CPW lines on the PCB and on the glass wafer. The measurements presented are carried out in the frequency range from 0.3 to 8 GHz at 20 °C. This packaging introduces transition elements, which can reduce the performances of the measurement. Same methodology of analysis was performed to estimate its influence on the results.

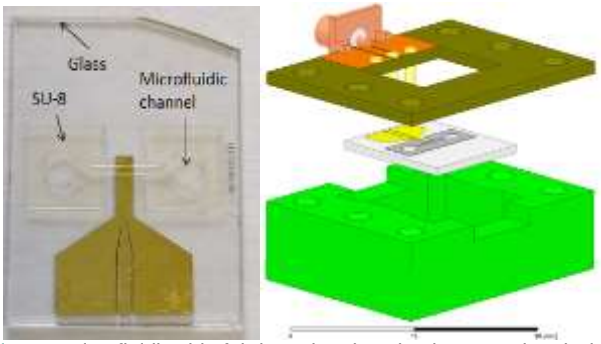

Fig. 17. Microfluidic chip fabricated and packaging associated with spring loaded contacts.

The reflection coefficient S_{11} is measured using the vector network analyzer. According to the measured media (air, deionized water, acetone, methanol and ethanol), the comparison of the measured and the fitted data, using the Debye model of complex dielectric permittivity of methanol and ethanol at 20°C is presented in Fig. 18 and Fig. 19, respectively. Table I summarizes the permittivity and relaxation frequencies of the Debye model obtained by fitting data and shows the differences in percent compared to the theoretical values. The measured and modeled data are very close to each other. This shows the relevance of the measurement and extracting methods.

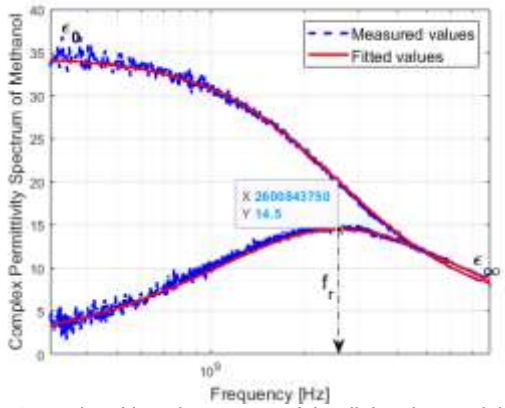

Fig. 18. Real and imaginary parts of the dielectric permittivity of methanol fitted or extracted from the measurement with connectorized sensor.

The advantage of this packaging technique is that the measurement system is made more flexible given the ease of using wired connections instead of under-probe protocol. After calibration, the dielectric properties of a large number of samples can be routinely measured in a short time as the measurement can be performed in a temperature-controlled environment without requiring any preparation of the sample.

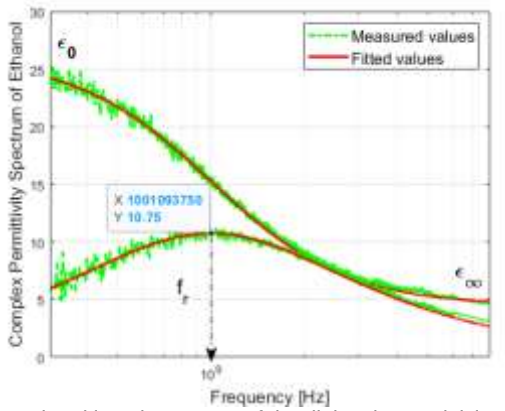

Fig. 19. Real and imaginary parts of the dielectric permittivity of ethanol fitted or extracted from the measurement with connectorized sensor.

TABLE I
VALUES OF THE PERMITTIVITIES AND RELAXATION FREQUENCIES OBTAINED BY FITTING DATA MEASURED WITH CONNECTORIZED SENSOR AT 293.15 K, WITH DEVIATION FROM EXPECTED VALUES IN BRACKETS.

Liquid	ε_s	ε_∞	f_r (GHz)
Methanol	32.83 (2.4%)	5.46 (3.4%)	2.60 (7.8%)
Ethanol	26.02 (3.4%)	4.58 (1.1%)	0.97 (17.8%)

B. Analysis of measurement reproducibility

In order to estimate the reproducibility of the previous results, measurement of ethanol and methanol properties have been performed four times, with a new liquid injection within the channel for each measurement. The four curves of extracted permittivity obtained in the case of ethanol are shown in Fig. 20(a). To highlight the deviation between the extracted values, the standard deviation between the four curves has been calculated at each frequency and normalized by the mean of these four values; the obtained normalized standard deviations for real and imaginary parts of the relative permittivity are plotted in Fig. 20(b). The obtained values stay below 14.5% over the all frequency range, the highest values obtained for the imaginary part at low frequencies corresponding to low mean values; the mean normalized standard deviation over the frequency range is of 1.24% for the real part and 1.73% for the imaginary part. In the case of methanol permittivity extraction using four different measurement results, the mean normalized standard deviation is of 2.85% for the real part and 3.53% for the imaginary part of the relative permittivity.

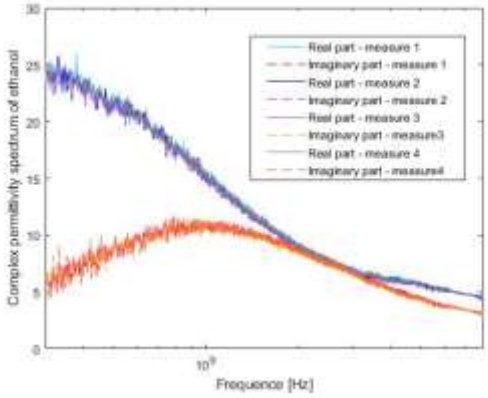

(a)

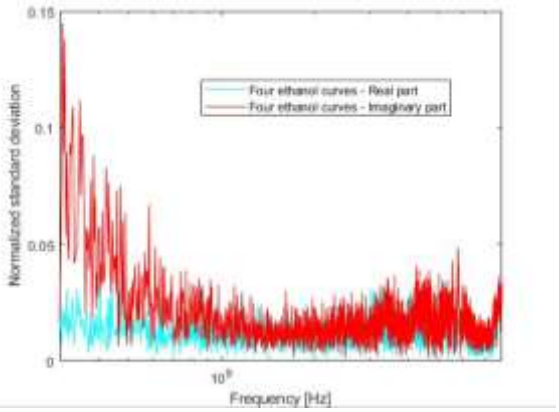

(b)

Fig. 20. Real and imaginary parts of the dielectric permittivity of ethanol extracted from four consecutive measurements with connectorized sensor (a), and the normalized standard deviation of the four curves of real and imaginary parts.

The curves of relative permittivity obtained from these four measurements have then been fitted according to Debye's model in order to extract the high and low frequency relative permittivity and the relaxation frequency associated to each measurement. Table II presents, for each of these three parameters, the mean of the four extracted values along with the normalized standard deviation between these four values. We can notice a good stability of the extracted parameters between the four measurements; the highest variation is obtained for the high frequency permittivity of methanol, the difficulty to extract this parameter being linked to the too low measurement frequency values.

TABLE II
MEAN AND NORMALIZED STANDARD DEVIATION OF THE EXTRACTED PERMITTIVITIES AND RELAXATION FREQUENCIES OBTAINED BY FITTING THE FOUR MEASUREMENT RESULTS WITH CONNECTORIZED SENSOR AT 293.15 K, WITH DEVIATION FROM EXPECTED VALUES IN BRACKETS.

Liquid	Indicator	ε_s	ε_∞	f_r (GHz)
Methanol	Mean value	34.06 (1.22%)	5.22 (7.75%)	2.68 (4.90%)
	Normalized standard deviation	4.70%	7.08%	2.43%
Ethanol	Mean value	26.22 (4.22%)	4.42 (2.43%)	0.984 (18.75%)
	Normalized standard deviation	1.71%	3.67%	5.93%

C. Mixtures of water and methanol measured by the SMA-connectorized sensor

To study and optimize the sensitivity of a biosensor, the impact of a liquid on the variation in the overall capacity of the sensor was evaluated. So, liquids with well-known permittivity have been used and mixed; here pure water and methanol.

The comparison of the measured real and imaginary parts of the complex dielectric permittivity of the analyzed of binary mixtures of water and methanol is presented in Fig. 21 and Fig. 22, respectively. The evolution versus frequency of the extracted complex permittivity of each mixture and of methanol are presented along with Debye models estimated from these extracted values and the theoretical model of the water. The device was calibrated considering three other reference media, namely air, deionized water and acetone.

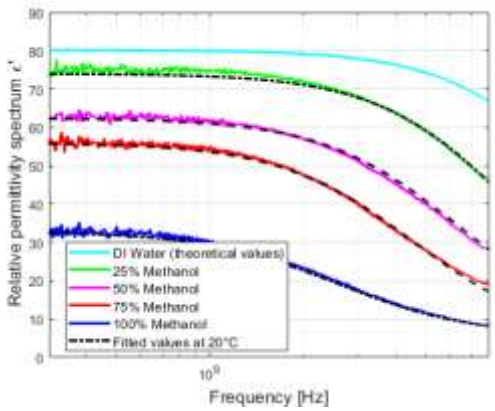

Fig. 21. Relative permittivity of water + methanol solutions measured at 293.15 K.

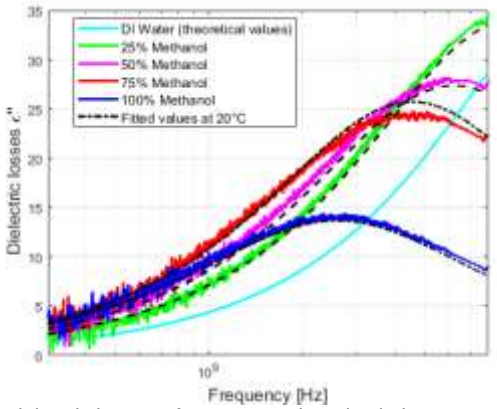

Fig. 22. Dielectric losses of water + methanol solutions measured at 293,15 K.

To evaluate the variation in the relaxation frequency, the difference was plotted between the parameters extracted from measurement and the theoretical values obtained using the equations described below as a function of the fraction volume [35]:

$$ln\, f_{mix} = X_1 ln f_1 + X_2 ln f_2 \quad (16)$$

where the indices 1 and 2 respectively represent the two solvents. X_1 and X_2 ($X_1 + X_2 = 1$) are the volume fractions of the respective components. Fig. 23 presents the dielectric relaxation frequencies of the mixtures f_T obtained from measurement and those obtained using (16).

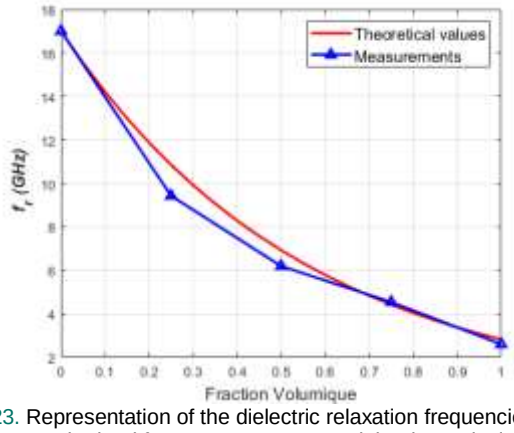

Fig. 23. Representation of the dielectric relaxation frequencies of the mixtures obtained from measurement and the theoretical model.

The theoretically derived results are compared with measurements carried out in the 0.2 - 25 GHz frequency range and show very good agreement on the relaxation frequency of the mixture. The dielectric relaxation parameters obtained by fitting the data are presented in Table III. The deviation in % with the specific analytical theoretical models is also given.

TABLE III
VALUES OF THE RELAXATION FREQUENCIES OBTAINED BY FITTING DATA MEASURED WITH CONNECTORIZED SENSOR AT 293.15 K

% Volumic proportion	f_r (GHz)
25% Methanol	17 (13.12%)
50% Methanol	9.42 (10.56%)
75% Methanol	6.19 (2.71%)
100% Methanol	4.54 (2.60%)
100% DI Water	2.60

VI. CONCLUSION

This paper is devoted to the developments of a miniaturized RF sensor for dielectric media characterization. The device operates in reflective mode with under-probe measurements. The results obtained, both by simulation and by experimental characterization, show that it is relevant to rely on microtechnologies to fabricate such a device combined with a dedicated procedure for dielectric parameter extraction.

The extraction method of the complex permittivity of liquid media, after a calibration step with three reference media, is proven to be functional. The measurement results are compared with those obtained using similar sensors but addressing much larger volumes. The complex permittivity extracted are very close to theoretical values.

The feasibility of detecting one microparticle within the media is also done (case of 20 µm microbeads). This result confirms the high interest of such sensor for biological cell analysis using their dielectric property in the RF range.

For portability purposes, a packaged version of the sensor with a SMA connector is proposed and leads to reliable results. It has been applied to mixture media analysis. These results are the first steps towards a simpler use of this type of sensor by avoiding under-probe measurements.

The prospects for applications of such a sensor, towards the characterization of heterogeneous media, concern the analysis of samples of a few nanoliters and containing a few biological cells. The media dielectric properties can be analyzed in order to detect the presence (or not) of a pathology (cell type, cancer, anemia,…) [36, 37].

References

[1] R. Baw and J. Finkelsetein, “Lab on a chip,” *Nature*, vol. 442, no. 7101, pp. 367–418, Jul. 2006.

[2] Dai, Li, et al. "Microfluidics-based microwave sensor." Sensors and Actuators A: Physical 309 (2020): 111910.

[3] N.Wagner, M. Schwing and A. Scheuermann, “Numerical 3-D FEM and Experimental Analysis of the Open-Ended Coaxial Line Technique for Microwave Dielectric Spectroscopy on Soil” IEEE Geoscience and Remote Sensing Society, 22 March 2013.

[4] Basics of measuring the dielectric properties of materials, Agilent Note, Agilent Technologies, 2006.

[5] Stuchly M. A., Brady M. M., Stuchly S. S., and Gajda G., “Equivalent circuit of an open-ended coaxial line in a lossy dielectric,” IEEE Trans. Instrum. Meas., vol. IM-31, no. 2, pp. 116–119, Jun. 1982.

[6] Stuchly M., Athey T., Samaras G., and Taylor G., “Measurement of radio frequency permittivity of biological tissues with an open-ended coaxial line: Part II—Expermental results,” IEEE Trans. Microw. Theory Tech., vol. 30, no. 1, pp. 87–92, Jan. 1982.

[7] Kraszewski A., Stuchly M. A., and Stuchly S., “ANA calibration method for measurements of dielectric properties,” IEEE Trans. Instrum. Meas., vol. 32, no. 2, pp. 385–387, Jun. 1983.

[8] Wei Y.-Z. and Sridhar S., “Radiation-corrected open-ended coax line technique for dielectric measurements of liquids up to 20 GHz,” IEEE Trans. Microw. Theory Tech., vol. 39, no. 3, pp. 526–531, Mar. 1991.

[9] Bao J. Z., Swicord M., and Davis C., “Microwave dielectric characterization of binary mixtures of water, methanol, and ethanol,” J. Chem. Phys., vol. 104, no. 12, pp. 4441–4450, Mar. 1996.

[10] Ulaby F., Bengal T., M. Dobson, J. East, J. Garvin, and D. Evans, “Microwave dielectric properties of dry rocks,” IEEE Trans. Geosci. Remote Sens., vol. 28, no. 3, pp. 325–336, May 1990.

[11] Lasne Y., Paillou P., Freeman A., Farr T., McDonald, Ruffie K. G., Malezieux J.-M., Chapman B., and Demontoux F., “Effect of salinity on the dielectric properties of geological materials: Implication for soil moisture detection by means of radar remote sensing,” IEEE Trans. Geosci. Remote Sens., vol. 46, no. 6, pp. 1674–1688, Jun. 2008.

[12] Sheen N. and Woodhead I., “An open-ended coaxial probe for broadband permittivity measurement of agricultural products,” J. Agricult. Eng. Res., vol. 74, no. 2, pp. 193–202, Oct. 1999.

[13] Skierucha W., Walczak R., and Wilczek A., “Comparison of open-ended coax and TDR sensors for the measurement of soil dielectric permittivity in microwave frequencies,” Int. Agrophys., vol. 18, no. 4, pp. 355–362, 2004.

[14] Van Damme S., Franchois A., De Zutter D., and Taerwe L., “Nondestructive determination of the steel fiber content in concrete slabs with an open-ended coaxial probe,” IEEE Trans. Geosci. Remote Sens., vol. 42, no. 11, pp. 2511–2521, Nov. 2004.

[15] Chen Y. and Or D., “Effects of Maxwell-Wagner polarization on soil complex dielectric permittivity under variable temperature and electrical conductivity,” Water Resour. Res., vol. 42, no. 6, p. W06424, Jun. 2006.

[16] Wagner N., Kupfer K., and Trinks E., “A broadband dielectric spectroscopy study of the relaxation behaviour of subsoil,” in Proc. 7th Int. Conf. Electromagn. Wave Interact. Water Moist Substances, 2007, pp. 31–38.

[17] Wagner N., Emmerich K., Bonitz F., and Kupfer K., “Experimental investigations on the frequency and temperature dependent dielectric material properties of soil,” IEEE Trans. Geosci. Remote Sens., vol. 47, no. 7, pp. 2518–2530, Jul. 2011.

[18] Mariam H., Poulichet P., Takhedmit H., Richalot E., Francais O., « Caractérisation des propriétés diélectriques de milieux liquides à l’aide d’une sonde à effet de bout sur une puce microfluidique », I2M-C2i, Oct 2019.

[19] Grenier K. et al., "Integrated Broadband Microwave and Microfluidic Sensor Dedicated to Bioengineering," IEEE

Transactions on Microwave Theory and Techniques, vol. 57, no. 12, pp. 3246-3253, Dec. 2009.

[20] Grenier K. et al., "Recent Advances in Microwave-Based Dielectric Spectroscopy at the Cellular Level for Cancer Investigations," IEEE Transactions on Microwave Theory and Techniques, vol. 61, no. 5, pp. 2023-2030, May 2013.

[21] Chen T., Dubuc D., Poupot M., Fournie J. and Grenier K., "Accurate Nanoliter Liquid Characterization Up to 40 GHz for Biomedical Applications: Toward Noninvasive Living Cells Monitoring," IEEE Transactions on Microwave Theory and Techniques, vol. 60, no. 12, pp. 4171-4177, Dec. 2012

[22] Vlachogiannakis, Gerasimos, et al. "Miniaturized broadband microwave permittivity sensing for biomedical applications." IEEE Journal of Electromagnetics, RF and Microwaves in Medicine and Biology 3.1 (2018): 48-55.

[23] Ning, Y., Multari, C., Luo, X., Palego, C., Cheng, X., Hwang, J. C., ... & Liberti, M. (2014). Broadband electrical detection of individual biological cells. IEEE Transactions on Microwave Theory and Techniques, 62(9), 1905-1911.

[24] Jonathan Leroy, Fatima Hjeij, Alaeddine Landoulsi, Carole Mélin, Claire Dalmay, Barbara Bessette, Christophe Bounaix, Morand Du Puch, Stéphanie Giraud, Christophe Lautrette, Serge Battu, Fabrice Lalloué, Marie-Odile Jauberteau-Marchan, Annie Bessaudou, Pierre Blondy, Arnaud Pothier, "Microfluidic Biosensors for Microwave Dielectric Spectroscopy", Sensors and Actuators A: Physical, Volume 229, Pages 172--181, Jun 2015. DOI: 10.1016/j.sna.2015.04.002

[25] T. Chen, D. Dubuc, M. Poupot, J-J. Fournié, K. Grenier, "Microwave biosensor dedicated to the dielectric spectroscopy of a single alive biological cell in its culture medium", IEEE International Microwave Symposium, Seattle, USA, June 2013. DOI: 10.1109/MWSYM.2013.6697740

[26] Wenli Chen, David Dubuc, Katia Grenier, "Microwave Dielectric Spectroscopy of a Single Biological Cell with Improved Sensitivity up to 40 GHz", DOI : 10.1109/MWSYM.2015.7166974

[27] Ma, Xiao, et al. "Sensitivity analysis for ultra-wideband 2-port impedance spectroscopy of a live cell." IEEE Journal of Electromagnetics, RF and Microwaves in Medicine and Biology 4.1 (2019): 37-44.

[28] Ma, Xiao, et al. "Ultra-wideband impedance spectroscopy of a live biological cell." IEEE Transactions on Microwave Theory and Techniques 66.8 (2018): 3690-3696.

[29] Ma, X., et al. "Broadband single-cell detection with a coplanar series gap." 2015 86th ARFTG Microwave Measurement Conference. IEEE, 2015.

[30] Mariam H., Poulichet P., Takhedmit H., Richalot E., Francais O., "Dielectric Spectroscopy Characterization within a Microfluidic Device based on Open-Ended Coplanar Waveguide", EuCAP, March 2020, Copenhagen

[31] Debye P. (1913). Ver. Deut. Phys. Gesell. 15, 777. Reprinted 1954 in collected papers of Peter J.W. Debye Interscience, New York.

[32] Debye P. (1929). Polar molecules. J. Soc. Chem. Ind., 48(43): 1036-1037.

[33] Marsland T., Evans S. (1987). Dielectric measurements with an open-ended coaxial probe. IEE Proceedings H Microwaves, Antennas and Propagation, 134(4): 341-349. http://dx.doi.org/10.1049/ip-h-2.1987.0068

[34] Bao J.Z., Davis C., Swicord, M. (1994). Microwave dielectric measurements of erythrocyte suspensions. Biophys. Soc. All Rights Res. Biphys. J., 66(6): 2173-2180. http://dx.doi.org/10.1016/S0006-3495(94)81013-6

[35] Lou J.F., Hatton T.A. and Laibinis P.E., J. Phys. Chem. A, 101, 5262 (1997).

[36] Hussein M., Awwad F., Jithin D., El Hasasna H., Athamneh K. & Iratni R. « Breast cancer cells exhibits specifc dielectric signature in vitro using the open-ended coaxial probe technique from 200MHz to 13.6GHz" 18 March 2019

[37] Khan U., Al-Moayed N., Nguyen N., Obol M., Korolev K., Afsar M. and Naber S., "High Frequency Dielectric Characteristics of Tumorous and Nontumorous Breast Tissues", 2007 IEEE/MTT-S Microwave Symposium, 2017, pp. 1341-1344.